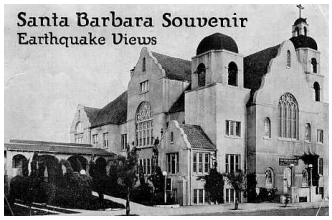

4th IASPEI / IAEE International Symposium:

Effects of Surface Geology on Seismic Motion

August 23–26, 2011 · University of California Santa Barbara

ENSEMBLE SIMULATIONS OF RUPTURES ON ROUGH FAULTS: VARIABILITY IN RUPTURE PROCESS AND GROUND MOTION

Zijun Fang
Department of Geophysics
Stanford University
Stanford, CA, 94305
USA

Hyunghoon Cho
Department of Computer Sciences
Stanford University
Stanford, CA, 94305
USA

Eric M. Dunham
Department of Geophysiccs
Stanford University
Stanford, CA, 94305
USA

ABSTRACT

Laboratory and field observations suggest that faults are self-similar surfaces with amplitude-to-wavelength ratios in the range of 10^{-3} to 10^{-2}. Motivated by these observations, we study spontaneous rupture propagation and the resulting ground motion for hundreds of random realizations of rough faults. Simulation results show that roughness causes significant fluctuations in rupture velocity and induces short-wavelength slip heterogeneity, which excite seismic waves over a broad range of wavelengths and result in an approximately ω^{-2} far-field displacement spectra. The remarkable similarity between the synthetic and observed seismograms suggests that rupture propagation on randomly generated self-similar faults could be a new and self-consistent way to generate synthetic ground motions that avoids the need to artificially combine deterministic low frequency simulations with stochastic high frequency time series. We also find that the rupture process can be rather complicated: bursts of supershear rupture occur on favorably oriented fault sections; occasionally, ruptures reverse their propagation direction and rupture a fault patch twice in a single event; sometimes, ruptures stop at geometrical barriers for seconds and then initiate again, all of which add complexities to ground motion predictions. We further use the representation theorem to calculate far-field body wave seismograms and Fourier spectra. For primarily unilateral ruptures, far-field radiation patterns change from a distinct double couple pattern with strong directivity effects at low frequencies to a more isotropic pattern with diminished directivity effects at high frequencies, suggesting that in addition to scattering along the wave propagation path, source effects may also be responsible for the observed frequency dependence of directivity effects.

INTRODUCTION

Laboratory and field measurements of natural fault surfaces suggest that fault surfaces are fractal and rough at all scales [e.g., Power and Tullis, 1991]. Slip on such faults induces stress changes that perturb the local stress field, causing inelastic deformation in the off-fault material in the near fault regions and increasing overall resistance to slip [Chester and Chester, 2000; Dieterich and Smith, 2009; Dunham et al., 2011b]. Such roughness-induced stress perturbations on faults cause rapid accelerations and decelerations in rupture speed and also lead to a heterogeneous slip distribution, both of which contribute to the generation of incoherent high frequency seismic waves [Hakell, 1964; Madriaga, 1977; Boore and Joyner, 1978; Spudich and Frazer, 1984; Dunham et al., 2011b].

Motivated by the observations of fault roughness, we study how roughness affects spontaneous rupture propagation and the resulting ground motion using the two-dimensional plane strain model proposed by Dunham et al. [2011a, b]. In current studies, we only focus on roughness scales down to a minimum wavelength $\lambda_{min} \sim 100$ m. This is sufficient to study the excitation of waves up to ~ 10 Hz, a typical upper limit of interest in earthquake engineering.

Previous studies indicate that at high frequencies, the far-field acceleration spectra are, to the first order approximation, band-limited white noise [Hanks, 1979; McGuire and Hanks, 1980; Hanks and McGuire, 1981]. In addition to local site effects and scattering along wave propagation paths, observations suggest that the source process itself becomes random at short wavelengths, and fluctuations in fault slip and rupture velocity show a stochastic character, which has served as the basis for a variety of ground motion simulation methods and earthquake source models.

Many existing approaches to generate synthetic seismograms involve development of stochastic source models, either kinematic or fully dynamic, but almost always with the assumption that faults are planar. Kinematic stochastic source models account for randomness by imposing a fractal slip distribution or building composite source models from fractal distributions of small events [e.g., Andrews, 1980, 1981; Herrero and Bernard, 1994; Zeng et al., 1994]. Dynamic source models typically impose stochastic distributions of initial stress or frictional parameters on flat faults [e.g., Andrews, 1980, 1981; Oglesby and Day, 2002; Guatteri et al., 2003; Ripperger et al., 2007]. Many of those imposed heterogeneities are regarded as proxies for unmodeled irregular fault geometries.

In our present work, we are able to directly account for geometric irregularities and the associated physical processes that are likely to occur for coseismic slip on rough surfaces. We have simulated earthquake rupture propagation on a large number of randomly generated rough faults. Random fault geometry causes random fluctuations in rupture velocity and induces short-wavelength slip heterogeneity, which results in an ω^{-2} far-field displacement spectra, consistent with observations from natural earthquakes. Using detailed rupture information (i.e., rupture velocity and rise times) from simulation results together with the representation theorem [Aki and Richards, 2002], we calculate far-field body wave seismograms and their Fourier spectra. These show that far-field radiation patterns change from a distinct double couple pattern with strong directivity effects at low frequencies to a more isotropic pattern with diminished directivity effects at high frequencies, suggesting that source effects may be an important factor in the observed frequency dependence of directivity effects. Our results also show that rupture propagation on rough faults can be rather complicated, which adds more uncertainties and complexities to ground motion predictions. In the following, we will first review laboratory and field measurements of fault roughness and then discuss the above three aspects of our findings in greater detail.

LABORATORY AND FIELD MEASUREMENTS OF FAULT ROUGHNESS

Anderson [1951] recognized that natural fault surfaces are not planar but irregular at all scales. Early field and laboratory measurements done by Brown and Scholz [1985], Power and Tullis [1988, 1991, 1995], and Lee and Bruhn [1996] concluded that natural fault surfaces are self-similar, meaning that they are statistically identical at all scales. Two common quantities used to describe fractal fault surfaces are the root mean square (rms) roughness and the power spectral density of roughness [e.g., Sagy et al., 2007].

Considering a one-dimensional fault profile in the form y = h(x), for a profile measured over length L, which includes all the wavelengths λ smaller than L, the rms roughness is defined as

$$h_{rms}(\lambda < L) = \sqrt{\frac{1}{L}\int_{-L/2}^{L/2} h^2(x)dx}\,. \tag{1}$$

For self-similar profiles, the rms roughness is independent of scale, which means that it is proportional to profile length L as

$$h_{rms}(L) = \alpha L, \tag{2}$$

in which α is the amplitude-to-wavelength ratio, which controls the severity of deviations from planarity.

Self-similar profiles have a power spectral density function $P_h(k)$ in a power law form:

$$P_h(k) = C_h|k|^{-\beta}, \tag{3}$$

where $k = 2\pi/\lambda$ is the wavenumber, C_h and β are constants with $\beta = 3$ for self-similar profiles [Berry and Lewis, 1980; Brown and Scholz, 1985; Scholz and Aviles, 1986; Power and Tullis, 1991]. By assuming ergodicity of fault profiles, Dunham et al. [2011b] defined a band-limited rms roughness between (positive) wavenumbers k_{min} and k_{max} as

$$h_{rms}(k_{\min}, k_{\max}) = \sqrt{\frac{1}{\pi}\int_{k_{\min}}^{k_{\max}} P_h(k)dk}\,, \tag{4}$$

from which, together with the power law expression of $P_h(k)$ and $k_{min} = 2\pi/L$, $k_{max} \rightarrow \infty$, the constant C_h can be expressed by the amplitude-to-wavelength ratio α as $C_h = (2\pi)^3\alpha^2$. Then, the power spectral density of a self-similar profile takes the form

$$P_h(k) = (2\pi)^3 \alpha^2 |k|^{-3}. \quad (5)$$

Measurements indicate that faults have larger α in the direction perpendicular to slip than in the direction parallel to slip. The slip-perpendicular direction, in which almost no cumulative slip occurs, usually has α values of ~10^{-2}, while the slip-parallel direction has measured α values in the range of 10^{-3} to 10^{-2}, with the lower bound representative of the roughness on mature faults [Power and Tullis, 1991]. Recent studies suggest that α decreases as faults accumulate more slip since wear processes tend to smooth fault surfaces [Sagy and Brodsky, 2009; Brodsky et al., 2011].

Recent studies [Renard et al., 2006; Sagy et al., 2007; Sagy and Brodsky, 2009; Candela et al., 2009; Brodsky et al., 2011] have performed high-resolution measurements of fault roughness in the range between ~10^{-5} m and ~ 10^{2} m. Their measurements indicate that fault surfaces are more likely to be self-affine rather than self-similar. However, currently there are no high-resolution data for roughness at scales above ~10^{2} m. In the meanwhile, some of these studies show that there is no single power spectral density function that can simultaneously fit data from all scales studied. Owing to the incomplete information, we choose to focus our discussion on self-similar faults.

HIGH FREQUENCY GROUND MOTION

We have studied rupture propagation on rough faults and the resulting ground motion using the two-dimensional fault model of Dunham et al. [2011a, b]. We first focus on strong ground motion in the near-source region. Figure 1 shows examples of synthetic seismograms and Fourier acceleration spectra from the same station (about 2 km from the fault) for several values of α, as well as the Lucerne Valley near-field strong ground motion record from the 1992 M_w 7.3 Landers, California earthquake. The Lucerne Valley site is about 2 km from the nearest fault segment [Wald and Heaton, 1994], and the record is widely considered to be representative of near-source strong ground motions from large subshear earthquake ruptures.

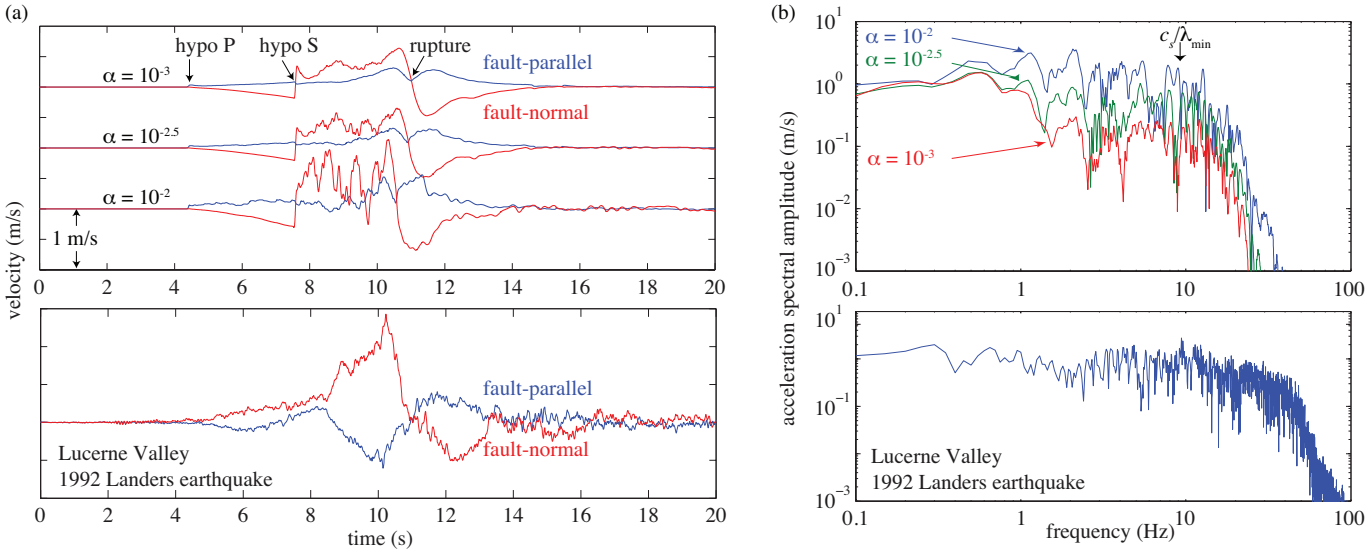

Fig 1. (a) Synthetic velocity seismograms (upper) for several values of amplitude-to-wavelength ratio α, with hypocentral P- and S-wave arrivals marked; Lucerne Valley record (lower) from the 1992 M_w 7.3 Landers earthquake. (b) Fourier amplitude spectra (FAS) of fault normal acceleration for the synthetic seismograms (upper) and the Lucerne Valley record (lower). The absence of roughness wavelengths smaller than λ_{min} prevents the excitation of waves at frequencies greater than ~c_s/λ_{min}.

As seen from Fig.1, although the synthetic seismograms are generated from a two-dimensional fault model, the main features of them are remarkably similar to those of the Lucerne Valley record: Beginning with the hypocentral P-wave arrival, the fault normal component experiences gradual increases in velocity in the direction toward the fault, which comes from the near-field and intermediate-field P-wave motions [Aki and Richards, 2002]. The absence of this feature in the Lucerne valley record is probably because of the significant changes in strike of the fault segments hosting the Landers earthquake or merely due to some instrumental correction [Chen, 1995]. Sustained strong motion in the fault normal direction begins with the hypocentral S-wave arrival and continues as shear waves ahead of the rupture front reach the station. The ground motion amplitudes are large during this period due to

forward directivity. Once the rupture passes the station, fault normal motion changes its direction and becomes much smaller due to backward directivity. Fig. 1 also shows that the amplitude of high frequency ground motion grows with increasing levels of roughness (i.e. larger values of α).

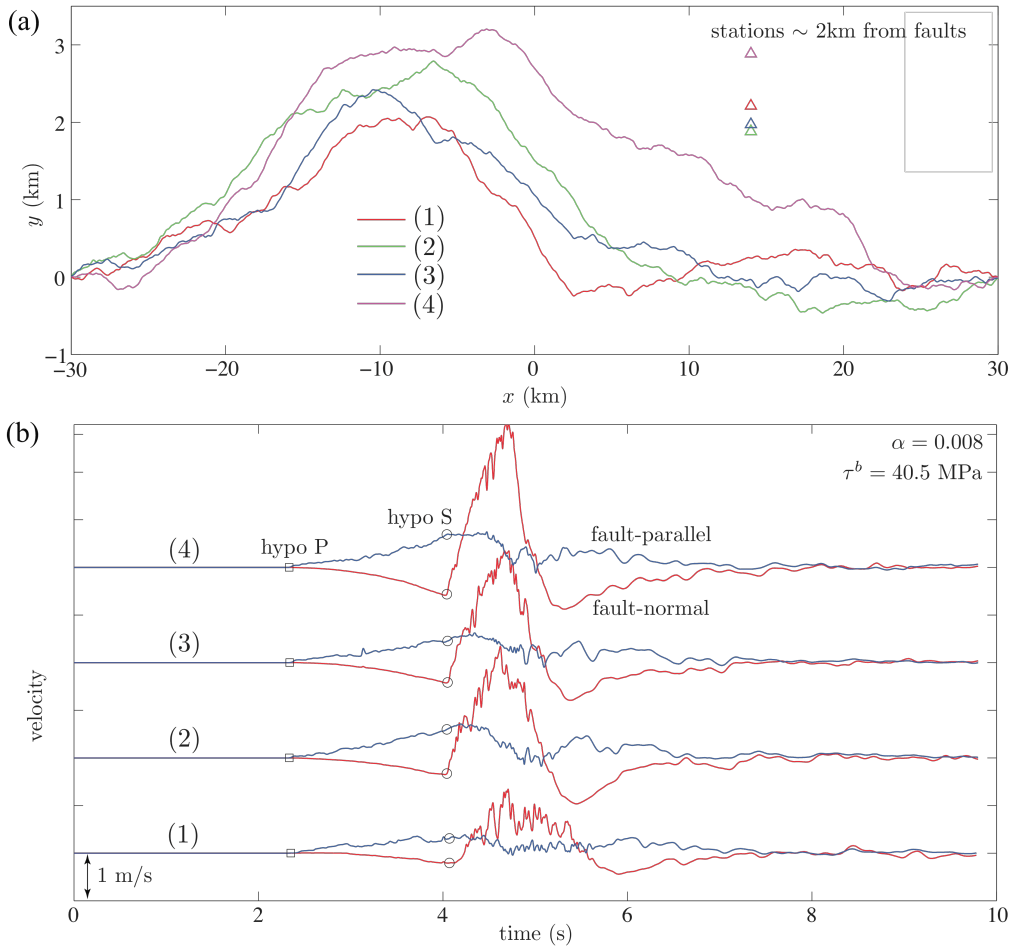

Fig.2: (a) Four realizations of self-similar fault profiles with identical values of the amplitude-to-wavelength ratio α. (b) Synthetic velocity seismograms for the four realizations of fault geometry shown in (a), demonstrating natural variability in ground motion.

As seen in Fig. 1, rupture propagation and ground motion are strongly dependent on fault geometry. We thus expect the rupture history and ground motion will not be the same for different realizations of the fault profile, even for profiles having identical amplitude-to-wavelength ratio α. This is demonstrated by Fig. 2. Figure 2(a) shows four different realizations of fault profiles with $\alpha = 0.008$. Synthetic seismograms are generated at four stations denoted by triangles, which are all about ~ 2 km from their corresponding fault profile (in the same color). From Fig. 2(b), it is obvious that while the general features are the same, the high frequency ground motions are quite different for the four cases. Case (1) has considerably smaller amplitudes than the other three cases simply because of its unique fault strike direction with respect to the station, which results in a smaller directivity effect. Additional variability arises when considering possible ranges of the initial shear stress level τ^b and the minimum wavelength of roughness λ_{min}. This study of near-field ground motion suggests that rupture propagation on randomly generated self-similar faults could be a new and self-consistent way to generate synthetic ground motions that avoids the need to artificially combine deterministic low frequency simulations with stochastic high frequency time series.

FAR FIELD GROUND MOTION

Observations [e.g., Bernard, 1994, 1996] suggest that directivity effects are generally only present at frequencies less than about 1 Hz, and at higher frequencies, the directivity effect vanishes and the far-field radiation pattern changes from the usual double-couple

pattern to an isotropic one. The differences in the directivity effect between high and low frequency ground motion have been alternatively explained as either a source effect (with the source losing coherence at short wavelengths) or a path effect (with high frequency waves being preferentially scattered by crustal heterogeneities).

In this paper, we study the contribution of source effects to the frequency dependence of far-field ground motion by constructing an approximate three-dimensional source model based on the rupture history (rupture velocity and rise times) from our two-dimensional simulations. The model is constructed by projecting the two-dimensional source onto a high-aspect-ratio fault under the assumption that the rupture process and nonplanar fault topography are everywhere the same across the smaller dimension (see Fig. 3(a) and 3(b)). We then calculate far-field body wave seismograms and Fourier spectra using the representation theorem [Aki and Richards, 2002]. As shown in Fig. 3(c) and 3(d), the synthetic seismograms for both P and S waves show clear directivity effects and a double-couple radiation pattern. As shown by Fig.4, the double couple pattern and directivity effects are most prominent at low frequencies and become diminished at high frequencies.

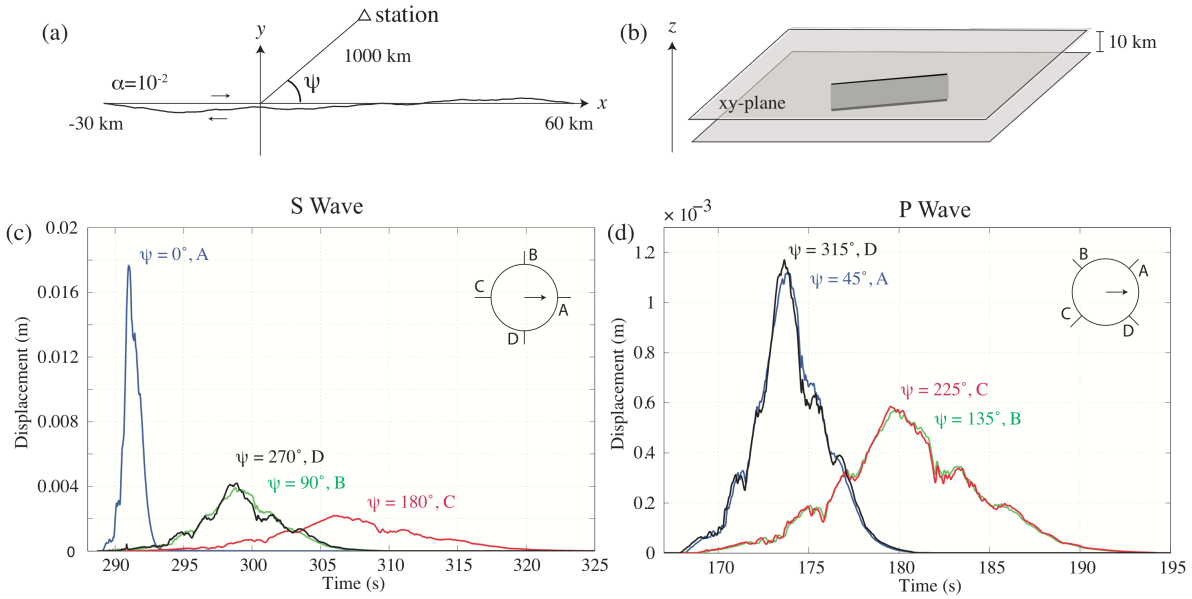

Fig.3: (a) The location of the station respect to the source. ψ is the angle between the station and x-axis. The station is assumed to be 1000 km from the hypocenter, which is considerably far compared to fault length ~100 km. (b) The two-dimensional fault used in our rupture simulations is simply elongated along the z-axis to obtain a three-dimensional fault surface, assuming that nonplanar topography is same everywhere along the z direction. (c) and (d) Calculated seismograms for S and P waves, respectively. Both show clear directivity effects and a double-couple radiation pattern.

This study suggests that the isotropic radiation pattern observed at high frequencies can be partially attributed to the source itself. Standard representations of source heterogeneity (spatially variable initial stress or friction parameters on flat faults) cannot capture the fluctuations in local radiation pattern on rough faults that causes the radiation pattern to become more isotropic at high frequencies.

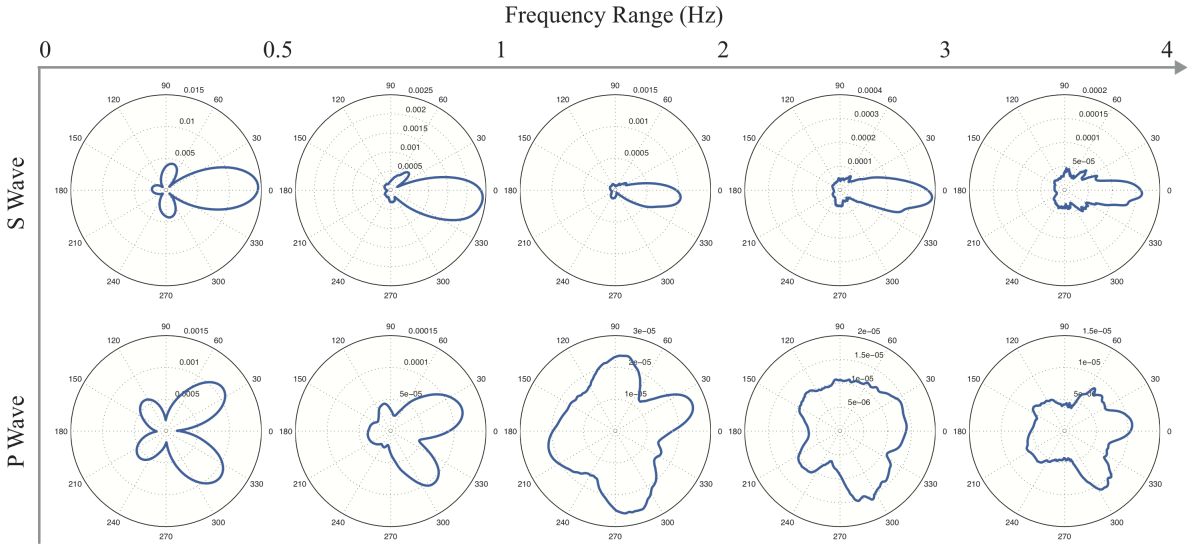

Fig.4: Radiation pattern for P- and S-waves at different range of frequencies. Starting from a clear double-couple pattern at low frequencies, the radiation pattern becomes more isotropic at higher frequencies because the local radiation pattern of each point on fault varies on rough faults. Directivity effects become weaker at high frequencies for both P and S waves, but do not disappear entirely for S waves.

COMPLEX RUPTURE BEHAVIORS

We model dynamic ruptures on rough faults using strongly rate-weakening fault friction, which is supported by many recent laboratory experiments [e.g., Tsutsumi and Shimamoto, 1997, Beeler et al., 2008]. One consequence of strongly rate-weakening friction is that, on flat fault models, for a range of initial stress conditions, ruptures occur as self-healing slip pulses instead of as cracks [e.g., Zheng and Rice, 1998]. Pulse-like rupture occurs as a slip pulse propagating along the fault, with cessation of slip behind the pulse, so that the slipping region occupies only a small width at the front of the expanding rupture zone, which can be clearly seen from Fig. 5(a) and 5(c).

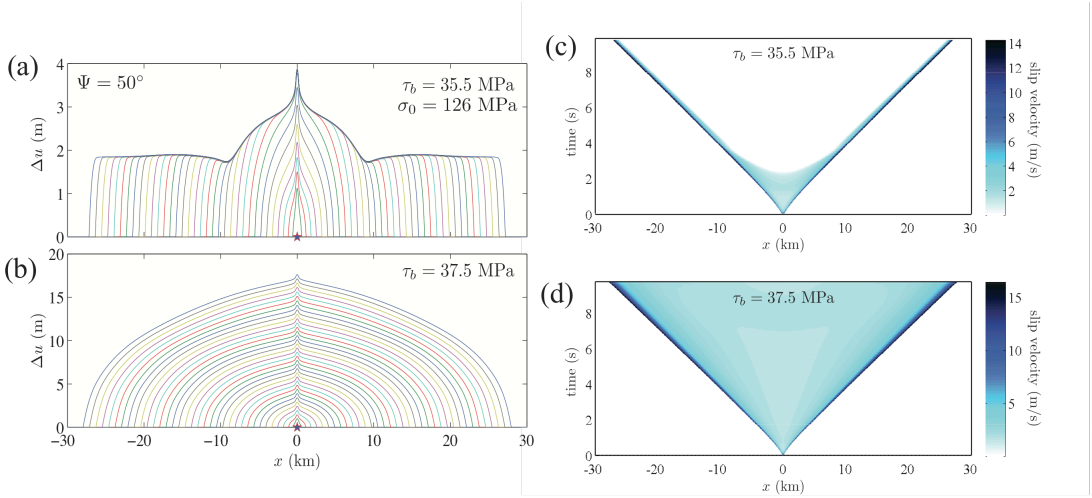

Fig.5: (a) and (b) Fault slip distribution for pulse-like and crack-like ruptures respectively. (c) and (d) Space-time plot of fault slip rate for pulse-like and crack-like ruptures. As shown by (c), pulse-like rupture starts from x = 0, t = 0 and propagates outward bilaterally. After ~2 s, nucleation region stops sliding. The rupture becomes a pulse, in that each point along the fault only slips for a duration ~0.2 s after rupture front passes by. As shown by (d), at higher stress levels, ruptures become expanding cracks, that is, while the rupture zone keeps expanding, slip continues growing everywhere within the rupture.

As seen from Fig. 5, in planar fault models, rupture processes are rather simple, taking either pulse-like or crack-like modes. In

contrast, rupture processes on rough faults can become rather complicated. In our simulations, we observe that bursts of supershear propagation that occurs when ruptures travel into high shear/normal stress regions, which often persists until the rupture encounters major geometrical barriers. Fig. 6(a) shows an example of a supershear burst, which is stopped by the geometric barrier at about 18 km. Notice that the sub-Rayleigh rupture front that arrives about 2 s later manages to pass through the barrier, leading to a much larger earthquake. In our simulations, we also observe 'backward ruptures', which re-rupture a fault section that has previously being ruptured. In the 2010 El Mayor-Cucapah earthquake [Fletcher, 2010] and the 2011 Tohoku-oki earthquake [Ide et al., 2011], there are lines of evidence suggesting that the rupture first goes in one direction then turns back to rupture in the opposite direction. Our results suggest that geometrical complexities can initiate these complex rupture histories.

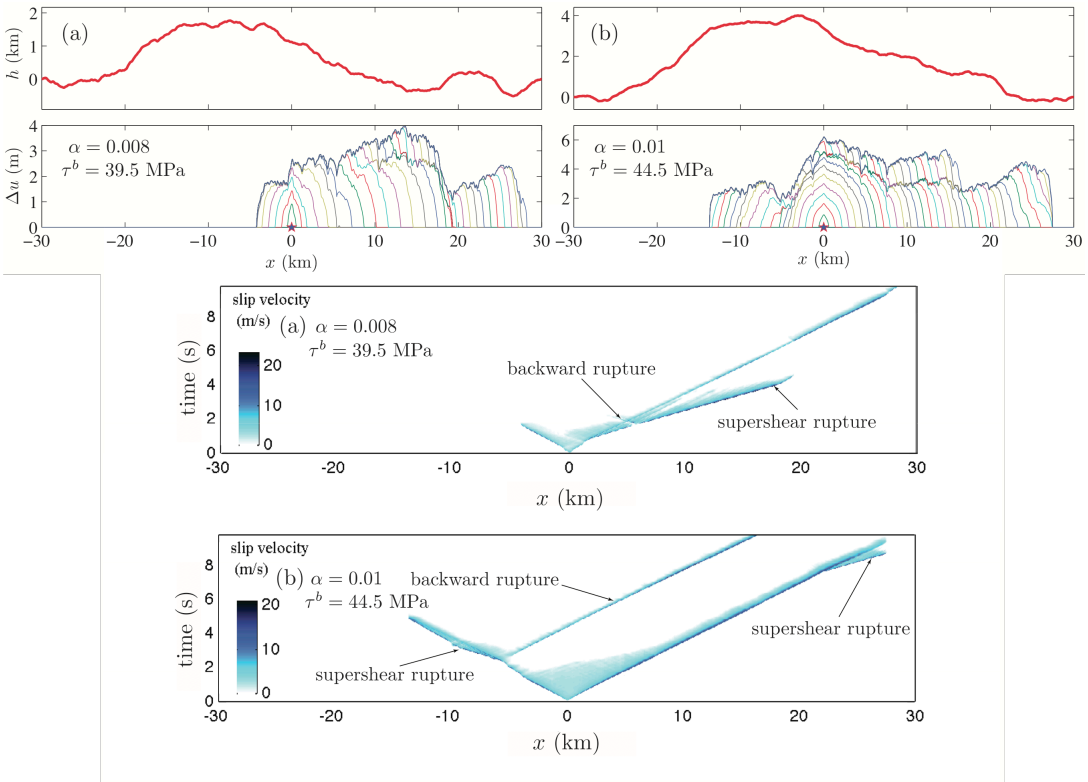

Fig.6: Complex rupture behaviors in our simulations of rupture propagation on randomly generated rough faults. (a) An example of a supershear burst. (b) An example of backward rupture.

CONCLUSIONS

We have used a two-dimensional model to simulate rupture propagation on a large number of randomly generated rough faults. The rough faults are band-limited self-similar fractal surfaces. Our simulation results show that fault roughness causes significant fluctuations in rupture velocity and induces short-wavelength slip heterogeneity, which contribute to the generation of high frequency ground motions that have an ω^{-2} far-field displacement spectra. The remarkable similarity between the synthetic and observed seismograms suggests that rupture propagation on randomly generated self-similar faults could be a new and self-consistent way to generate synthetic ground motions for earthquake engineering purposes. Using the representation theorem and the source information provided by our simulations, we calculated far-field body wave seismograms and Fourier spectra, which show that the far-field radiation patterns change from a distinct double couple pattern with strong directivity effects at low frequencies to a more isotropic pattern with diminished directivity effects at high frequencies, suggesting that in addition to scattering along the propagation path, source effects may also be responsible for the observed frequency dependence of directivity effects. We also find that the rupture process can be rather complicated on rough faults. We observe frequent short bursts of supershear rupture on favorably oriented fault sections, occasionally ruptures can even reverse their propagation direction and rupture a fault patch twice in a single event. All of these add complexities to ground motion predictions.

REFERENCES

Aki, K., and P. Richards (2002), *Quantitative Seismology*, University Science Books, Sausalito, California.

Andrews, D. J. (1980), A stochastic fault model, 1. Static case, *J. Geophys. Res.*, *85*, 3867–3877.

Andrews, D. J. (1981), A stochastic fault model, 2. Time-dependent case, *J. Geophys. Res.*, *86* (B11), 10,821–10,834.
Bernard, P., and A. Herrero, Slip heterogeneity, body wave spectra and directivity of earthquake ruptures, *Annali di Geofisica*, *47*(6), 1679–1690.

Beeler, N. M., T. E. Tullis, and D. L. Goldsby (2008), Constitutive relationships and physical basis of fault strength due to flash heating, *J. Geophys. Res.*, *113*, B01401, doi:10.1029/2007JB004988.

Bernard, P., A. Herrero, and C. Berge (1996), Modelling directivity of heterogeneous earthquake ruptures, *Bull. Seism. Soc. Am.*, *86* (4), 1149–1160.

Boore, D. M., and W. B. Joyner (1978), The influence of rupture incoherence on seismic directivity, *Bull. Seism. Soc. Am.*, *68* (2), 283–300.

Brown, S. R., and C. H. Scholz (1985), Broad bandwidth study of the topography of natural rock surfaces, *J. Geophys. Res.*, *90* (B14), 12,575–12,582.

Brodsky, E.E., J. J. Gilchrist, A. Sagy, and C. Collettini (2011), Faults smooth gradually as a function of slip, *Earth Planet. Sci. Lett.*, *302*, 185–193, doi:10.1016/j.epsl.2010.12.010.

Candela, T., F. Renard, M. Bouchon, A. Brouste, D. Marsan, J. Schmittbuhl, and C. Voisin (2009), Characterization of fault roughness at various scales: Implications of three-dimensional high resolution topography measurements, *Pure Appl. Geophys.*, *166* (10), 1817–1851, doi:10.1007/s00024-009-0521-2.

Chen, X. (1995), Near-field ground motion from the Landers earthquake, *Tech. Rep. CaltechEERL:1995.EERL-95-02*, California Institute of Technology.

Chester, F. M., and J. S. Chester (2000), Stress and deformation along wavy frictional faults, *J. Geophys. Res.*, *105*, 23,421–23,430.

Dieterich, J. H., and D. E. Smith (2009), Nonplanar faults: Mechanics of slip and off-fault damage, *Pure Appl. Geophys.*, *166* (10), 1799–1815, doi:10.1007/s00024-009-0517-y.

Dunham, E. M., D. Belanger, L. Cong, and J. E. Kozdon (2011a), Earthquake ruptures with strongly rate-weakening friction and off-fault plasticity: 1. Planar faults, *Bull. Seism. Soc. Am.*, *in press*.

Dunham, E. M., D. Belanger, L. Cong, and J. E. Kozdon (2011b), Earthquake Ruptures with Strongly Rate-Weakening Friction and Off-Fault Plasticity: 2. Nonplanar Faults, *Bull. Seism. Soc. Am.*, *in press*.

Fletcher, J. (2010), Distribution and kinematics of surface ruptures associated with the El Mayor-Cucapah earthquake sequence (invited talk), *SCEC Annual Meeting, Proceedings and Abstracts, Volume XX*, p. 213.

Guatteri, M., P. M. Mai, G. C. Beroza, and J. Boatwright (2003), Strong ground motion prediction from stochastic-dynamic source models, *Bull. Seism. Soc. Am.*, *93* (1), 301–313.

Hanks, T. C. (1979), b values and ω^{-2} seismic source models: Implications for tectonic stress variations along active crustal fault zones and the estimation of high-frequency strong ground motion, *J. Geophys. Res.*, *84* (B5), 2235–2242, doi:10.1029/JB084iB05p02235.

Hanks, T. C., and R. K. McGuire (1981), The character of high-frequency strong ground motion, *Bull. Seism. Soc. Am.*, *71* (6), 2071–2095.

Hartzell, S., S. Harmsen, A. Frankel, and S. Larsen (1999), Calculation of broadband time histories of ground motion: Comparison of methods and validation using strong-ground motion from the 1994 Northridge earthquake, *Bull. Seism. Soc. Am.*, *89* (6), 1484–1504.

Haskell, N. A. (1964), Total energy and energy spectral density of elastic wave radiation from propagating faults, *Bull. Seism. Soc. Am.*, *54* (6), 1811–1841.

Herrero, A., and P. Bernard (1994), A kinematic self-similar rupture process for earthquakes, *Bull. Seism. Soc. Am.*, *84* (4), 1216–1228.

Ide, S., A. Baltay and G. C. Beroza (2011), Shallow dynamic overshoot and energetic deep rupture of the 2011 Mw 9.0 Tohoku-Oki earthquake, Science, doi:10.1126/science.1207020.

Lee, J.-J., and R. L. Bruhn (1996), Structural anisotropy of normal fault surfaces, *J. Struct. Geol.*, *18* (8), 1043–1059.

Madariaga, R. (1977), High-frequency radiation from crack (stress drop) models of earthquake faulting, *Geophys. J. Roy. Astr. Soc.*, *51*, 625–651.

McGuire, R. K., and T. C. Hanks (1980), RMS accelerations and spectral amplitudes of strong ground motion during the San Fernando, California earthquake, *Bull. Seism. Soc. Am.*, *70* (5), 1907–1919.

Oglesby, D. D., and S. M. Day (2002), Stochastic fault stress: Implications for fault dynamics and ground motion, *Bull. Seism. Soc. Am.*, *92*, 3006–3021.

Power, W. L., and T. E. Tullis (1988), Roughness and wear during brittle faulting, *J. Geophys. Res.*, *93* (B11), 15,268–15,278.

Power, W. L., and T. E. Tullis (1991), Euclidean and fractal models for the description of rock surface roughness, *J. Geophys. Res.*, *96* (B1), 415–424.

Power, W. L., and T. E. Tullis (1995), Review of the fractal character of natural fault surfaces with implications for friction and the evolution of fault zones, in *Fractals in the Earth Sciences*, C. C. Barton and P. R. L. Pointe, chap. 5, pp. 89–105, Plenum Press.

Renard, F., C. Voisin, D. Marsan, and J. Schmittbuhl (2006), High resolution 3D laser scanner measurements of a strike-slip fault quantify its morphological anisotropy at all scales, *Geophys. Res. Lett.*, *33*, L04305, doi:10.1029/2005GL025038.

Ripperger, J., J.-P. Ampuero, P. M. Mai, and D. Giardini (2007), Earthquake source characteristics from dynamic rupture with constrained stochastic fault stress, *J. Geophys. Res.*, *112*, B04311, doi:10.1029/2006JB004515.

Sagy, A., E. E. Brodsky, and G. J. Axen (2007), Evolution of fault-surface roughness with slip, *Geology*, *35* (3), 283–286, doi:10.1130/G23235A.1.

Sagy, A., and E. E. Brodsky (2009), Geometric and rheological asperities in an exposed fault zone, *J. Geophys. Res.*, *114*, B02301, doi:10.1029/2008JB005701.

Scholz, C. H. and C. A. Aviles, The fractal geometry of faults and faulting, in *Earthquake Source Mechanics*, edited by S. Das, J. Boatwright and C. H. Scholz, *Geophys. Monogr.*, vol. *37*, pp. 147–155, AGU, Washington, D. C., 1986.

Spudich, P., and L. N. Frazer (1984), Use of ray theory to calculate high frequency radiation from earthquake sources having spatially variable rupture velocity and stress drop, *Bull. Seism. Soc. Am.*, *74*, 2061–2081.

Tsutsumi, A., and T. Shimamoto (1997), High velocity frictional properties of gabbro, *Geophys. Res. Lett.*, *24*, 699–702.

Wald, D. J., and T. H. Heaton (1994), Spatial and temporal distribution of slip for the 1992 Landers, California, earthquake, *Bull. Seism. Soc. Am.*, *84* (3), 668–691.

Zeng, Y., J. G. Anderson, and G. Yu (1994), A composite source model for computing realistic synthetic strong ground motions, *Geophys. Res. Lett.*, *2*(8), 725–728.

Zheng, G., and J. R. Rice (1998), Conditions under which velocity-weakening friction allows a self-healing versus a crack-like mode of rupture, *Bull. Seism. Soc. Am.*, *88*, 1466–1483.